Experimental Validation of a Combined Electromagnetic and Thermal Model for a Microwave Drying of Capillary Porous Materials Inside a Rectangular Wave Guide (Effects of Irradiation Time, Particle Sizes and Initial Moisture Content)

P. Ratanadecho, K. Aoki and M. Akahori

In this paper, the experimental validation of a combined electromagnetic and thermal model for a microwave drying of capillary porous materials inside a rectangular wave guide is presented. The effects of the irradiation time, particle sizes and the variation of initial moisture content on the microwave drying kinetics are clarified in detail, considering the interference between incident and reflected waves in the capillary porous materials. The established model has allowed us to determine the space-time evolution of electric field, temperature and moisture content within capillary porous materials during microwave drying process.

Key Words: Microwave drying, Capillary Porous Materials, Rectangular Wave Guide, FDTD, Dielectric Properties.

ABOUT THE AUTHORS:
Phadungsak Ratanadecho is affiliated with the Department of Mechanical Engineering, Thammasat University, Thailand. Kazuo Aoki and Masatoshi Akahori, are affiliated with the Department of Mechanical Engineering, Nagaoka University of Technology, Nagaoka, Niigata, Japan.

From a theoretical standpoint, the drying process of porous media is a complicated process involving simultaneous, coupled heat and mass transfer phenomena. A multitude of experimental and theoretical work has been done in this area and a lot of applications exist in different technological areas such as drying of foods, drying of paper, freeze drying process, vulcanization of rubber and medical applications.

Microwave interacts with individual molecules to quickly generate heat within a product. Consequently, when properly designed, microwave-heating systems have several advantages over conventional mechanical methods such as shorter processing times for heating or drying, volumetric dissipation of energy throughout a product, high energy efficiency compared with conventional drying, and offer improvements in product quality for various industrial applications. Metaxas and Meredith [1983] and Saltiel and Datta [1997] provide good introduction to heat and mass transfer in microwave processing.

Recently, many excellent studies in this area have discussed the importance of mathematical modeling on understanding the complex phenomenon that arises during microwave drying of porous materials. Perkin et al. [1980] developed the heat and mass transfer model to describe the drying of unbound, pendular moisture, by a method utilizing the volumetric absorption of microwave energy generated at radio or microwave frequency. Gori et al. [1987] studied the microwave drying of soil layer by using the Lambert's law, in their work, the agreement between the numerical predictions and experimental results for moisture and temperature profiles seems to be quite acceptable.

The work of Wei et al. [1985], Turner and Jolly [1990], Turner and Jolly [1991], and Turner et al. [1998], which is a low microwave power process that typically generates low pressure, and most math-

ematical models have been solved for microwave drying using finite difference method and the control volume method. Chen and Schmidt [1990] studied microwave drying of hygroscopic and nonhygroscopic materials using an integral method that divided the computational zone into a two-region problem, a wet zone and sorption zone. Ratanadecho et al. [2001a] studied the drying process of unsaturated porous materials inside a microwave oven, they emphasized the effect of particle size and initial moisture content on the drying kinetics.

Furthermore, intensive microwave drying has been studied by Constant et al. [1996] and Ni et al. [1999]. In the study conducted by Constant et al. [1996], the microwave power absorbed term in the mathematical model was determined from the actual experiment. They found that in the case of high microwave power drying, the liquid expulsion mechanism was developed from both the experimental and numerical standpoints.

Ni et al. [1999] developed one-dimensional model to predict moisture transport under intensive microwave heating of biomaterials, with transport properties that can change with changes in structure, moisture and temperature.

However, most previous investigations are replete with one-dimensional drying model and the microwave power absorbed was assumed to decay exponentially into the sample following the Lambert's law. Although this assumption is valid for the sample thick enough to be treated as infinitely thick ($L_{crit} \approx 3 \times$ penetration depth where the penetration depth or distance at which the incident electric field has decayed by a factor of 1/e of its incident intensity), it is a poor approximation in many practical situations [Ayappa et al., 1991].

For the small sample heats in a faster rate by microwave due to the resonance of standing waves whereas resonance is completely absent for greater length scales. In perspective, Lambert's exponential decay law cannot predict resonance. Therefore, the spatial variations of the electromagnetic field within small samples must be obtained by solution of the Maxwell's equations [Ratanadecho et al., 2001b].

In some more recent work, the microwave drying process of solid materials (soft wood) inside an oversized wave guide was studied by Perre and Turner [1997], the model that was based on Whitaker's theory, took into account the difference of the transport mechanism with respect to various kinds of the sample.

Ratanadecho et al. [2001c] presented the microwave drying of capillary porous packed bed by using a rectangular wave guide, the effects of transmitted and reflected waves and the variation of microwave power level and particle sizes on drying kinetics at shorter drying times were studied systematically.

This work describes the characteristics of microwave drying at 2.45GHz in the TE_{10} mode of capillary porous materials. Furthermore, from the macroscopic point of view, the effects of the particle size and initial moisture content on the overall drying kinetics at longer drying times is also clarified in this work. The specific objectives of this work are to:

- formulate the generalized mathematical model of the microwave drying process,
- solve the mathematical model numerically,
- compare the numerical results with experimental measurements.

The results presented here provide a basis for fundamental understanding of microwave drying of dielectric materials.

Experimental Apparatus

Figure 1(a) shows the experimental apparatus used. The microwave system was a monochromatic wave of TE_{10} mode operating at a frequency of 2.45GHz. Microwave energy was generated by magnetron (Micro Denshi Co., Model UM-1500), it was transmitted along the z-direction of the rectangular wave guide with inside dimensions of 110 mm × 54.61 mm toward a water load that was situated at the end of the wave guide. The water load (lower absorbing boundary) ensured that only a minimal amount of microwave was reflected back to the sample. Also, an isolator (upper absorbing boundary) was used to trap any microwave reflected from the sample to prevent it from damaging the magnetron (Figure 1(b)). Output of magnetron was adjusted to 50 W.

During the experiment, the microwave field was

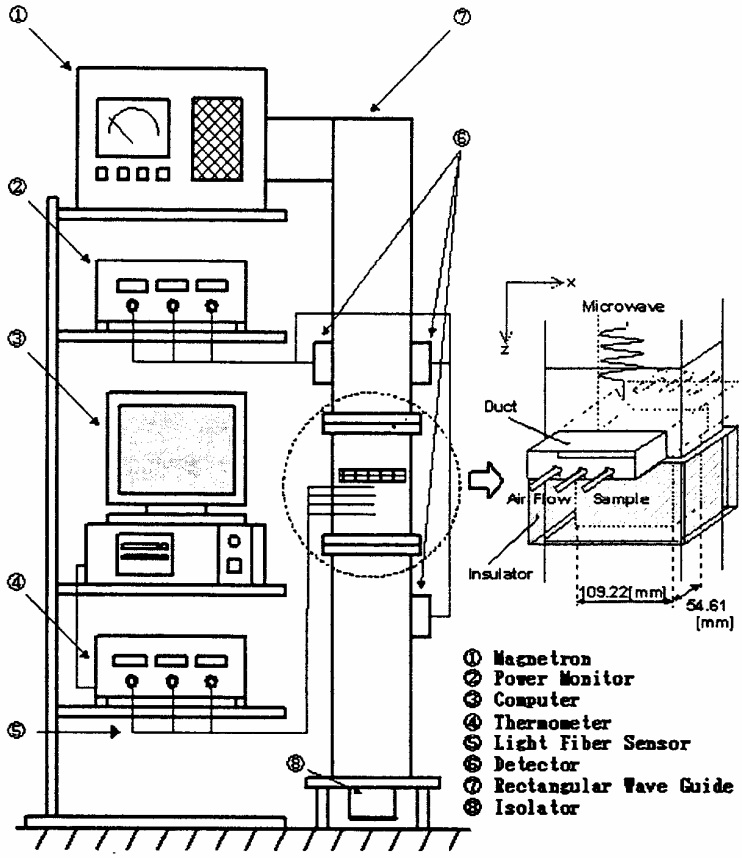

(a)

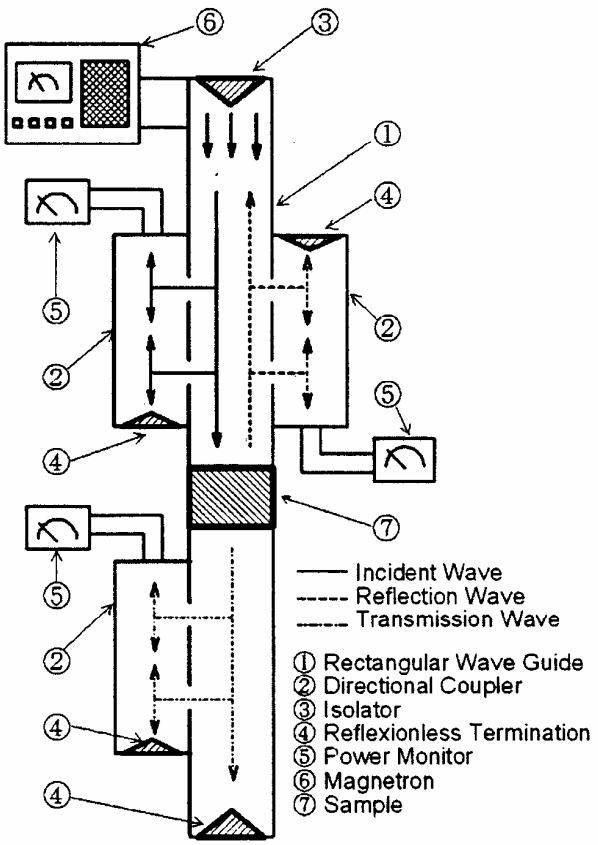

(b)

FIGURE 1: *Schematic of experimental facility:*

(a) Equipment setup;

(b) Microwave measuring system

generated using a magnetron (Micro Denshi Co., Model UM-1500). The powers of incident, reflected and transmitted waves were measured by wattmeter using a directional coupler (Micro Denshi Co., Model DR-5000). The distributions of temperature within the sample were measured using fiberoptic (LUXTRON Fluroptic Thermometer, Model 790, accurate to ± 0.5°C), which were placed in the center of the sample at each 5 mm interval. An infrared camera was also used to measure the temperature distributions within the sample in x-z plane.

The sample studied was a packed bed of 50mm in thick, which was comprised of glass beads and water. The samples were prepared in two kinds: a saturated porous packed bed (s_0=1.0 and d=0.15 mm, d=0.4 mm and d=1.0 mm) and unsaturated porous packed bed (s_0=0.6 and d=0.15 mm), it was inserted perpendicular to direction of irradiation via a rectangular wave guide. A sample container made of polypropylene was 0.75 mm in thickness, it did not absorb microwave energy.

During the experimental microwave drying processes, the uncertainty of our data might came from the variations in humidity, room temperature and human errors. The calculated drying kinetic uncertainties in all tests were less than 3 percent. The uncertainty in temperature was assumed to result from errors in measured input power, ambient temperature and ambient humidity. The calculated uncertainty associated with temperature was less than 2.85 percent.

Analysis of Mathematical Modeling

Generally, studies on the microwave drying involve solutions of the equations governing electromagnetic propagation, i.e., Maxwell's equations, either by themselves or coupled with the heat and mass transport equations. A two-dimensional physical model in the x-z plane is presented in Figure 2.

Analysis of Electromagnetic Model

Figure 2 shows the physical model for microwave

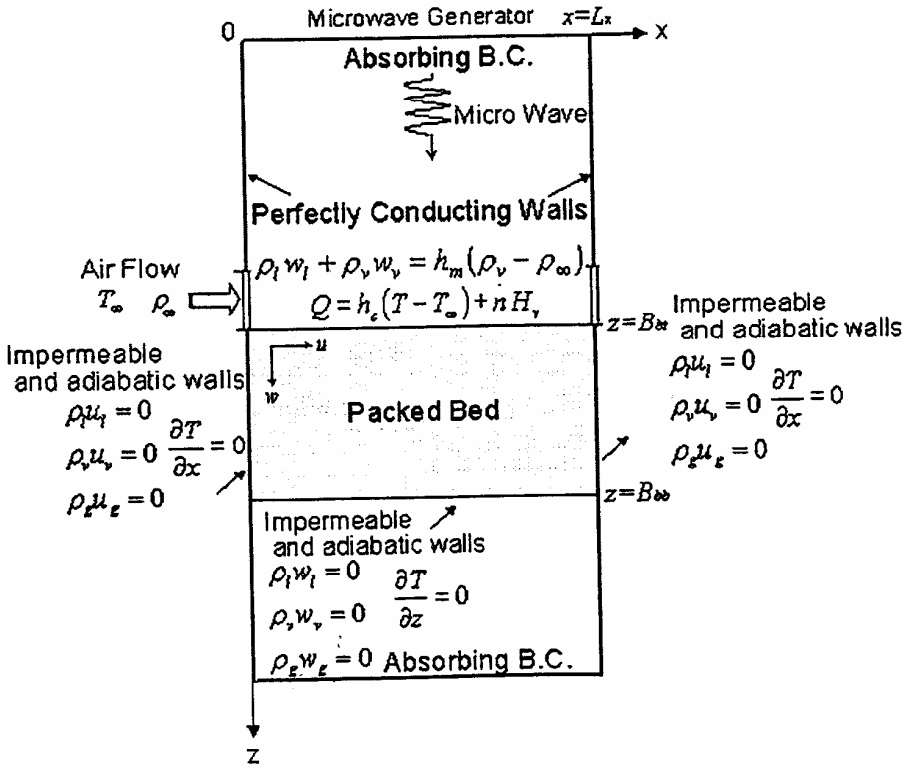

FIGURE 2: Physical model.

drying of capillary porous materials using a rectangular wave guide. The proposed model is based on the following assumptions [Ratanadecho et al, 2001d]:

- Since the microwave field is operated in TE_{10} mode, it propagates in a rectangular wave guide independently of the y-direction. Hence the electromagnetic field can be assumed to be two-dimensional plane (x-z plane).
- The absorption of microwave energy by the cavity (including air) in the rectangular wave guide is negligible.
- The walls of a rectangular wave guide are perfect conductors.
- The effect of the sample container on the electromagnetic field can be neglected.

The basic equations for the electromagnetic field are based on the well-known Maxwell relations. When a microwave field propagates through an isotropic medium having permittivity ε, magnetic permeability μ, electric conductivity σ, and electric charge density q, the governing equations are given as follows:

$$\nabla \times \boldsymbol{E} = -\mu \frac{\partial \boldsymbol{H}}{\partial t} \tag{1}$$

$$\nabla \times \boldsymbol{H} = \sigma \boldsymbol{E} + \frac{\partial \boldsymbol{E}}{\partial t} \tag{2}$$

$$\nabla \cdot \boldsymbol{E} = \frac{q}{\varepsilon} \tag{3}$$

$$\nabla \cdot \boldsymbol{H} = 0 \tag{4}$$

For the microwave of TE_{10} mode, the components of electric and magnetic field intensities are given by:

$$\begin{aligned} E_x = E_z = H_y = 0 \\ E_y, H_x, H_z \neq 0 \end{aligned} \tag{5}$$

where subscripts x, y and z represent x, y and z components of vectors, respectively. Using the relation of Equation 5, the governing equations (Equations (1)-(4)) can be written in terms of the component notations of electric and magnetic field intensities [Ratanadecho et al, 2001b]:

$$\frac{\partial E_y}{\partial z} = \mu \frac{\partial H_x}{\partial t} \tag{6}$$

$$\frac{\partial E_y}{\partial x} = -\mu \frac{\partial H_z}{\partial t} \tag{7}$$

$$-\left(\frac{\partial H_z}{\partial x} - \frac{\partial H_x}{\partial z}\right) = \sigma E_y + \varepsilon \frac{\partial E_y}{\partial t} \tag{8}$$

where, permittivity ε, magnetic permeability μ and electric conductivity σ are given by:

$$\varepsilon = \varepsilon_0 \varepsilon_r \tag{9}$$

$$\mu = \mu_0 \mu_r \tag{10}$$

$$\sigma = 2\pi f \varepsilon \tan \delta \tag{11}$$

where f is frequency of microwave, $\tan \delta$ is dielectric loss tangent, ε_r and μ_r are relative permittivity or dielectric loss factor and relative magnetic permeability, respectively. In addition, if magnetic effects are negligible, which is true for most dielectric materials used in microwave heating applications, the magnetic permeability (μ) is well approximated by its value μ_0 in the free space.

Further, the dielectric properties are assumed to vary with temperature and moisture content during drying processes. The dielectric properties utilized throughout this study use a mixing formula which can be found in literature [Wang et al., 1980]

Boundary Conditions

Corresponding to the physical model as shown in Figure 2, boundary conditions can be given as follows:

(a) Perfectly conducting boundaries: Boundary conditions on the inner wall surface of a rectangular wave guide are represented by Faraday's law

and Gauss' theorem:

$$E_t = 0, \; H_n = 0 \tag{12}$$

where subscripts t and n denote the components of tangential and normal directions, respectively.

(b) Continuity boundary condition: Boundary conditions along the interface between different materials, for example between air and dielectric material surface, are represented by Ampere's law and Gauss' theorem:

$$E_t = E'_t, \quad H_t = H'_t$$
$$D_n = D'_n, \quad B_n = B'_n \tag{13}$$

(c) Absorbing boundary condition: At both ends of the rectangular wave guide, the first order absorbing conditions proposed by Mur [1981] are applied:

$$\frac{\partial E_y}{\partial t} = \pm \upsilon \frac{\partial E_y}{\partial z} \tag{14}$$

Here, the symbol ± represents forward or backward waves and υ is phase velocity of the microwave.

(d) Oscillation of the electric and magnetic flied intensities by magnetron: Incident wave due to magnetron is given by the following equations:

$$E_y = E_{yin} \sin\left(\frac{\pi x}{L_x}\right) \sin(2\pi f t) \tag{15}$$

$$H_x = \frac{E_{yin}}{Z_H} \sin\left(\frac{\pi x}{L_x}\right) \sin(2\pi f t) \tag{16}$$

E_{yin} is the input value of electric field intensity, L_x is the length of rectangular wave guide in x-direction, Z_H is the wave impedance defined as:

$$Z_H = \frac{\lambda_g Z_l}{\lambda_0} = \frac{\lambda_g}{\lambda_0} \sqrt{\frac{\mu_0}{\varepsilon_0}} \tag{17}$$

where Z_l denotes intrinsic impedance depending on the properties of material. λ_0 and λ_g are wave length of microwaves in free space and rectangular wave guide, respectively.

Analysis of Heat and Mass Transport Models

The samples considered are packed beds of glass beads in either water and air which are then modeled as homogeneous and isotropic structures, these materials are selected to demonstrate the model, because most of its physical properties are well documented.

A schematic diagram of the model is shown in Figure 2. By conservations of mass and energy in the sample, the governing equations of mass and energy for all phases can be derived by using the volume average technique [Whitaker, 1977]. The main transport mechanism for the moisture movement during microwave drying of the sample are: liquid flow is driven by capillary pressure gradient and gravity while the vapor is driven by the gradient of the partial pressure of the evaporating species.

Due to the complexity of the phenomena, and difficulty of finding actual situations in which the main assumptions involved in the formulation are [Ratanadecho et al., 2001c]:

- The capillary porous material is rigid. No chemical reactions occur in the sample.
- Local thermodynamic equilibrium is assumed.
- Simultaneous heat and mass transport occurs at constant pressure, where the dominant mechanisms are capillary transport, vapor diffusion and gravity. Such is generally the case in drying of capillary porous medium at atmospheric pressure when the temperature is lower than the boiling point [Bories, 1991].
- The contribution of convection to energy transport is included.
- Corresponding to electromagnetic field, temperature and moisture profiles also can be assumed to be two-dimension in the x-z plane.

The governing equations based on a volume average approach lead to the following conservation equations describing the drying process of capillary porous material:

Mass Conservation

$$\phi\frac{\partial}{\partial t}\{\rho_l s+\rho_v(1-s)\}+\frac{\partial}{\partial x}[\rho_l u_l+\rho_v u_v]+\frac{\partial}{\partial z}[\rho_l w_l+\rho_v w_v]=0 \quad (18)$$

Energy Conservation

$$\frac{\partial}{\partial t}\left[\left(\rho c_p\right)_T T\right]+\nabla\left[\left\{\rho_l c_{pl}\boldsymbol{u}_l+\left(\rho_a c_{pa}+\rho_v c_{pv}\right)\boldsymbol{u}_g\right\}T\right]+H_v\dot{n}=-\nabla q+Q \quad (19)$$

where H_v is the latent heat of vaporization of water and Q is the local electromagnetic heat generation term, which is a function of the electric field distribution and defined as [Clemens et al., 1996 and Ratanadecho et al., 2001c]:

$$Q=2\pi\cdot f\cdot\varepsilon_0\cdot\varepsilon_r(\tan\delta)E_y^2 \quad (20)$$

Phenomenological Relations

In order to obtain the system of equations, above, the expressions for the superficial average velocity of the liquid and gas phases based on the generalized Darcy's law in the following vector form is used:

$$\boldsymbol{u}_l=-\frac{\boldsymbol{K}K_{rl}}{\mu_l}\left[\nabla p_g-\nabla p_c-\rho_l\boldsymbol{g}\right] \quad (21)$$

$$\boldsymbol{u}_g=-\frac{\boldsymbol{K}K_{rg}}{\mu_g}\left[\nabla p_g-\rho_g\boldsymbol{g}\right] \quad (22)$$

the velocity of vapor water and air phases based on the generalized Fick's law for two components gas mixture can be expressed in vector form as:

$$\rho_v\boldsymbol{u}_v=\rho_v\boldsymbol{u}_g-\rho_g D_m\nabla\left(\frac{\rho_v}{\rho_g}\right) \quad (23)$$

$$\rho_a\boldsymbol{u}_a=\rho_a\boldsymbol{u}_g-\rho_g D_m\nabla\left(\frac{\rho_a}{\rho_g}\right) \quad (24)$$

where the capillary pressure p_C is related to the gas and liquid phases:

$$p_c=p_g-p_l \quad (25)$$

and D_m is the effective molecular mass diffusion [Rogers et al., 1992]:

$$D_m=\frac{2\phi}{3-\phi}(1-s)D_0 \quad (26)$$

Fourier's law is used to define the heat flux through the porous medium:

$$q=-\lambda_{eff}\nabla T \quad (27)$$

Equilibrium Relations

The system of conservation equations obtained for multiphase transport mode requires constitutive equation for relative permeabilities K_r, capillary pressure p_C, capillary pressure functions (Leverett functions) J, and the effective thermal conductivity λ_{eff}. A typical set of constitutive relationships for liquid and gas system is given by:

$$K_{rl}=s_e^3 \quad (28)$$

$$K_{rg}=\left(1-s_e\right)^3 \quad (29)$$

where s_e is the effective water saturation considered the irreducible water saturation s_{ir} and is defined by

$$s_e = \frac{s - s_{ir}}{1 - s_{ir}} \tag{30}$$

The capillary pressure p_C is further assumed to be adequately represented by Leverett's well-known $J(s_e)$ functions, the relationship between the capillary pressure and the water saturation is defined by using Leverett functions $J(s_e)$:

$$p_c = p_g - p_l = \frac{\xi}{\sqrt{K/\phi}} J(s_e) \tag{31}$$

in which ξ is the gas-liquid interfacial tension, where $J(s_e)$ was correlated capillary pressure data obtained by Leverett as follows to give $J(s_e)$:

$$J(s_e) = 0.325(1/s_e - 1)^{0.217} \tag{32}$$

Figure 3 shows the typical moisture characteristic curve for different particle sizes obtained from previous work of Ratanadecho et al. [2001a]. It is seen that, in the case of the same water saturation, a small particle size corresponds to a higher capillary pressure.

Figure 4 shows the effective thermal conductivity λ_{eff} of capillary porous materials obtained from previous work of Ratanadecho et al. [2001a] and can be written in empirical form as:

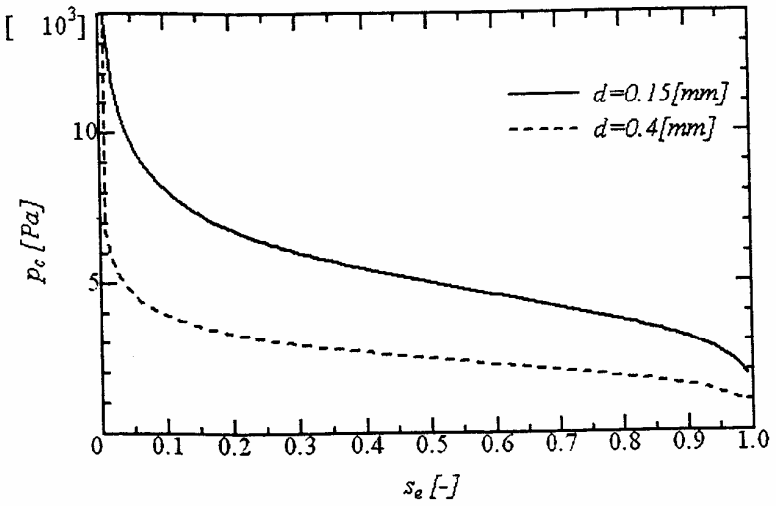

FIGURE 3: Typical relationship between, p_c *and* s_e.

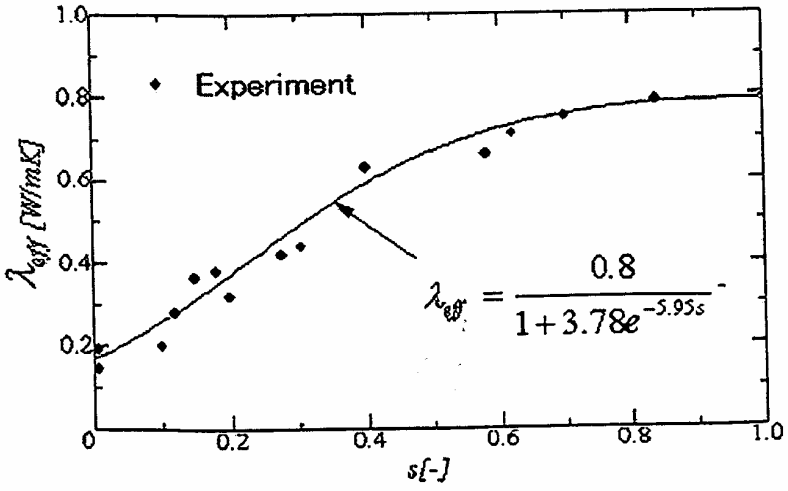

FIGURE 4: Thermal properties of porous materials.

$$\lambda_{eff} = \frac{0.8}{1+3.78e^{-5.95s}} \tag{33}$$

State Equations

The gas phase is assumed to be an ideal mixture of perfect gas, so that the species density can be determined by the state equations, with the classical definitions for total density of the gas ρ_g and the mass average velocity of the gas:

$$\rho_a = \frac{p_a M_a}{R_0 T}, \rho_v = \frac{p_v M_v}{R_0 T}, \rho_g = \rho_a + \rho_v,$$
$$p_a = \rho_a R_a T, p_v = \rho_v R_v T, p_g = p_a + p_v, \rho_g u_g = \rho_a u_a + \rho_v u_v \tag{34}$$

After some mathematical manipulations [Ratanadecho et al., 2001c], the two-dimensional system of two non-linear coupled partial differential equations for the drying process are given by:

Moisture Transport Equation

$$\phi \frac{\partial}{\partial t}\{\rho_l s + \rho_v(1-s)\} + \frac{\partial}{\partial x}\left[\rho_l \frac{KK_{rl}}{\mu_l}\left(\frac{\partial p_c}{\partial x}\right) - D_m \frac{\partial \rho_v}{\partial x}\right]$$
$$+\frac{\partial}{\partial z}\left[\rho_l \frac{KK_{rl}}{\mu_l}\left(\frac{\partial p_c}{\partial z} + \rho_l g_z\right) + \rho_v \frac{KK_{rg}}{\mu_g}\left(\rho_g g_z\right) - D_m \frac{\partial \rho_v}{\partial z}\right] = 0 \tag{35}$$

Heat Transport Equation

$$\frac{\partial}{\partial t}\left[\left(\rho c_p\right)_T T\right] + \frac{\partial}{\partial x}\left[\left\{\rho_l c_{pl} u_l + \left(\rho_a c_{pa} + \rho_v c_{pv}\right)u_g\right\}T\right] + \frac{\partial}{\partial z}\left[\left\{\rho_l c_{pl} w_l + \left(\rho_a c_{pa} + \rho_v c_{pv}\right)w_g\right\}T\right] + H_v \dot{n}$$
$$= \frac{\partial}{\partial x}\left[\lambda_{eff}\frac{\partial T}{\partial x}\right] + \frac{\partial}{\partial z}\left[\lambda_{eff}\frac{\partial T}{\partial z}\right] + Q \tag{36}$$

$$\left(\rho C_p\right)_T = \rho_l C_{pl}\phi s + \left\{\left(\rho C_p\right)_a + \left(\rho C_p\right)_v\right\}\phi(1-s) + \rho_p C_{pp}(1-\phi) \tag{37}$$

Also, the phase change term is given by

$$\dot{n} = \frac{\partial}{\partial t}\{\rho_v \phi(1-s)\} + \frac{\partial}{\partial x}\left[-D_m \frac{\partial \rho_v}{\partial x}\right] + \frac{\partial}{\partial z}\left[\rho_v \frac{KK_{rg}}{\mu_g}\rho_g g_z - D_m \frac{\partial \rho_v}{\partial z}\right] \tag{38}$$

where (rC_p) is the effective heat capacitance of water-gas-matrix mixtures.

Boundary and Initial Conditions

The boundary conditions proposed for the exchange of energy and mass transport at the open boundary can be described in the following form:

$$-\lambda_{eff}\frac{\partial T}{\partial z} = h_c(T - T_\infty) + \dot{n}H_v \tag{39}$$

$$\rho_l w_l + \rho_v w_v = h_m(\rho_v - \rho_\infty) \tag{40}$$

Considering the boundary conditions at the closed boundary that no heat and mass exchange take place:

$$\frac{\partial T}{\partial x} = \frac{\partial T}{\partial z} = 0, \frac{\partial u}{\partial x} = \frac{\partial w}{\partial z} = 0 \tag{41}$$

The initial conditions are given by uniform initial temperature and moisture.

Numerical Solution Procedure

The descriptions of heat and moisture transport equations (Equations (35) and (36)) are coupled to the Maxwell equations (Equations (6)-(8)) by Equation (20). The later equation represents the heating effect of microwaves within the sample. The numerical schemes of the microwave drying process are performed.

Electromagnetic Field Equations and FDTD Discretization

Generally, simulation of microwave power dissipation requires the solution of the set of three couple scalar partial differential equations governing electromagnetic propagation, i.e., Maxwell's equation, inside a rectangular wave guide. The finite difference time-domain (FDTD) method has been used to provide a full description of electromagnetic scattering and absorption and give detail spatial and temporal information of wave propagation.

In this study, the leapfrog scheme is applied to set of Maxwell's equations. The electric field vector components are offset one half cell in the direction of their corresponding components, while the magnetic field vector components are offset one half cell in each direction orthogonal to their corresponding components [Clemens et al., 1996]. The electric field and magnetic field are evaluated at alternative half time steps. For TE mode, the electric and magnetic field components are expressed the total field FDTD equations as:

$$E_y^n(i,k) = \frac{1-\dfrac{\sigma(i,k)\Delta t}{2\varepsilon(i,k)}}{1+\dfrac{\sigma(i,k)\Delta t}{2\varepsilon(i,k)}} E_y^{n-1}(i,k) + \frac{1}{1+\dfrac{\sigma(i,k)\Delta t}{2\varepsilon(i,k)}} \frac{\Delta t}{\varepsilon(i,k)} \left\{ \frac{-\left(H_z^{n-1/2}(i+1/2,k) - H_z^{n-1/2}(i-1/2,k)\right)}{\Delta x} + \frac{\left(H_x^{n-1/2}(i,\, k+1/2) - H_x^{n-1/2}(i,\, k-1/2)\right)}{\Delta z} \right\} \tag{42}$$

$$H_x^{n+1/2}(i,k+1/2) = H_x^{n-1/2}(i,k+1/2) + \frac{\Delta t}{\mu(i,k+1/2)} \left\{ \frac{E_y^n(i,k+1) - E_y^n(i,k)}{\Delta z} \right\} \tag{43}$$

$$H_z^{n+1/2}(i+1/2,k) = H_z^{n-1/2}(i+1/2,k) - \frac{\Delta t}{\mu(i+1/2,k)} \left\{ \frac{E_y^n(i+1,k) - E_y^n(i,k)}{\Delta x} \right\} \tag{44}$$

Heat and Moisture Transports Equations and Finite Control Volume Discretization

The coupled non-linear set of Equations (35)-(41) are solved numerically by using the finite control volume method [Patankar, 1980]. The basic strategy of finite control volume discretization method is to divide the calculated domain into a number of control volumes and then integrate the conservation equations over this control volume over an interval of time [t,t + Δt] . At the boundaries of the calculated domain, the conservation equations are discretized by integrating over half the control volume and by taking into account the boundary conditions. At the corners of the calculated domain, we used a quarter of control volume. At each time increment, the nodal values of s and T were solved iteratively and convergence was checked on both variables. The Newton-Raphson method was employed at each iteration for quicker convergence.

The Stability and Accuracy of Calculation

The choice of spatial and temporal resolution is motivated by reasons of stability and accuracy. Equations (35)-(41) are solved on a grid system, and temporally they are solved alternatively for both the electric and magnetic fields (Equations (6)-(8)). To insure stability of the time-stepping algorithm Δt must be chosen to satisfy the courant stability condition and defined as:

$$\Delta t \leq \frac{\sqrt{(\Delta x)^2 + (\Delta z)^2}}{\upsilon} \qquad (45)$$

and the spatial resolution of each cell , defined as:

$$\Delta x, \Delta z \leq \frac{\lambda_g}{10\sqrt{\varepsilon_r}} \qquad (46)$$

Corresponding to Equations (45) and (46), the calculation conditions are as follows:

- grid size: dx = dz = 1.0 mm,
- since the propagating velocity of microwave is so fast compared with the rate of heat transfer, different time steps of $\Delta t = 1 \times 10^{-12}$ s and $\Delta t = 0.1$ s are used corresponding to electromagnetic field and temperature field calculations, respectively.
- number of grid: N = 110 (width) × 200 (length),
- a prespecified stopping criterion for the iteration procedures of 10^{-8} were chosen.

Some of the input data for electromagnetic and thermo physical properties and drying conditions are given in Table 1 and Table 2, respectively.

Results and Discussion

Simulation of Electric Field in a Rectangular Wave Guide

In the beginning, to understand the detailed structures of electric field developed inside a rectangular wave guide, the numerical simulation of the following three cases are conducted:

(1) Rectangular wave guide is empty, its dielectric constant is unity (which corresponds to that of air).

(2) Rectangular wave guide is filled with sample with drying times of 15 min (early drying times).

(3) Rectangular wave guide is filled with sample with drying times of 540 min (long drying times).

Figures 5-7 are the numerical simulation of the distribution of electric field in TE_{10} mode inside a rectangular wave guide as well as the sample. In the figures, the vertical axis represents the intensity of the electric field E_y , which is normalized to the amplitude of the input electromagnetic wave, E_{yin}. However, all figures show the moment when the electric field attains its maximum.

Figure 5 shows the stationary wave inside the rectangular wave guide with completely absorbed power at the end of the rectangular wave guide (case 1). It is observed that the electric field distribution displays a wavy behavior with an almost uniform amplitude along a rectangular wave guide. Figure 6 shows the wave distribution of electric field when a dielectric material or sample is inserted in the rect-

TABLE 1: The electromagnetic and thermo physical properties used in the computations.

ε_0=8.85419×10^{-12}[F/m]
ε_0=1.0,
μ_{ra}=1.0,
tanδ_a=0.0,
ρ_a=1.205[kg/m^3]
C_{pa}=1.007[kJ/(kg K)],
ε_{rl}=88.15–0.4147=(0.131×10^{-2})T^2–(0.046×10^{-4})T^3

μ_0=4.0π×10^{-7}[H/m]
ε_{rp}=5.1
μ_{rp}=1.0,
tan δ_p=0.01 μ_{rl}=1.0
ρ_p=2500.0[kg/m^3], ρ_l=1000.0[kg/m^3]
C_{pp}=0.80[kJ/kg K)], C_{pl}=4.186[kJ/kg K)]
tan δ_l=0.323 – (9.499×10^{-3})T+(1.27×10^{-4})T^2–(6.13×10^{-7})T^3

TABLE 2: The drying conditions used in the computations.

Drying Conditions	Value
Glass bead sizes, d[mm]	0.15, 0.4, 1.0
Porosity, ϕ	0.385, 0.371
Initial saturation, S_0	0.99, 0.6
Initial temperature, T_0 [°C]	10.0
Irreducible saturation, S_{ir}	0.06
Air temperature, T_∞ [°C]	10.0
Air velocity, U_∞ [m/s]	5.0
Microwave power level, P[W]	50.0

angular wave guide (case 2). Within the sample (100mm ≤ z ≤ 150 mm), the electric field attenuates owing to energy absorption, and thereafter the absorbed energy is converted to the thermal energy, which increases the sample temperature. In the figure, the electric field within the sample is almost extinguished, however, focusing attention of field pattern outside the sample (left hand side, 0 mm ≤ z ≤ 100 mm), a stronger standing waves with a large amplitude is formed by interference between the forward wave and reflected wave from the surface of sample due to the different of dielectric properties of material (air and sample) at this surface.

Figure 7 shows the wave distribution of the electric field when a dielectric material or sample is inserted in the rectangular wave guide (case 3). In this case after a majority of the moisture level inside the sample has been removed, the effect of reflected wave from the surface of sample is reduced which increases the large part of microwaves penetrating

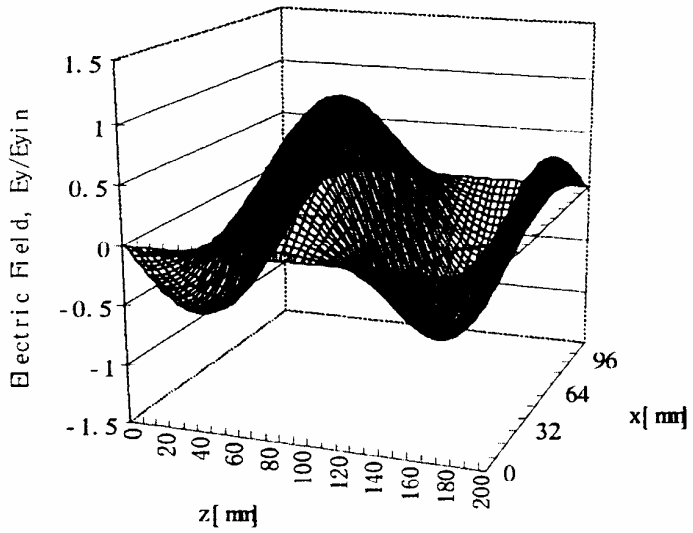

FIGURE 5: Distribution of electric field for case of a rectangular wave guide is empty (x=54.61 mm).

FIGURE 6: Distribution of electric field for case of sample is inserted in the rectangular wave guide (t=15 min, x = 54.61 mm).

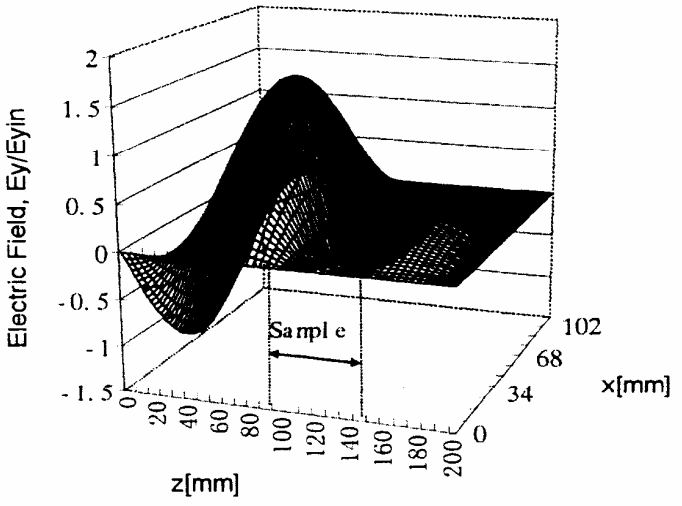

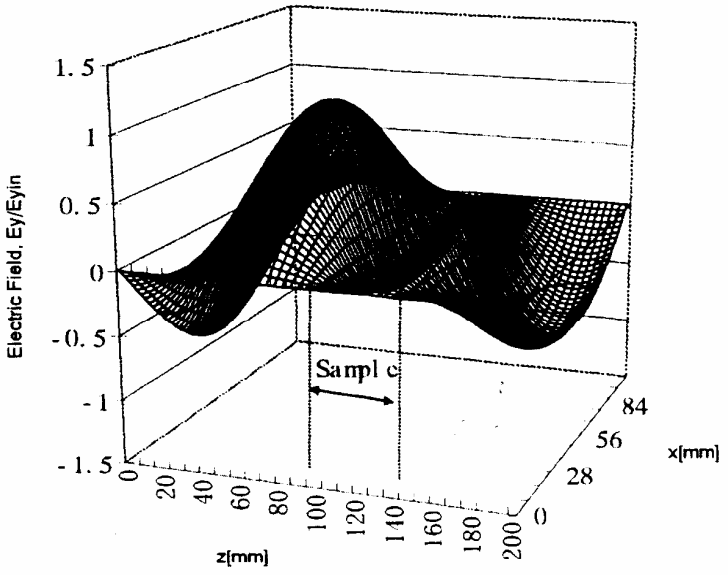

FIGURE 7: Distribution of electric field for case of sample inserted in the rectangular wave guide (t=540 min, x=54.61 mm).

the sample. Consequently, the reflection and transmission components at each interface will contribute to the resonance of standing waves configuration with the larger amplitude inside the sample compared with previous cases.

The Distribution of Temperature Profiles Within the Sample

The predicted results are compared with experimental microwave drying data in Figures 8 through 11,

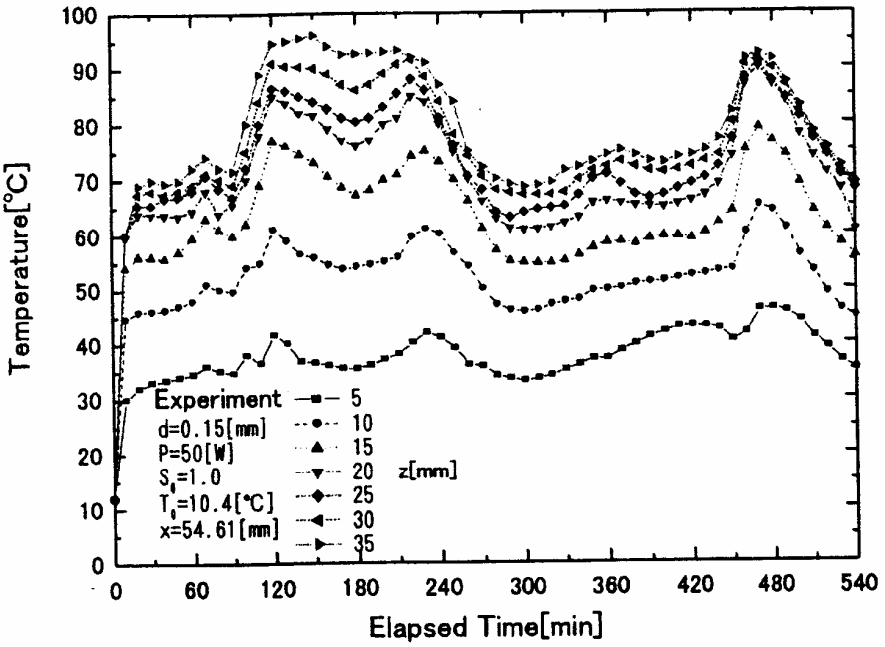

(a)

(b)

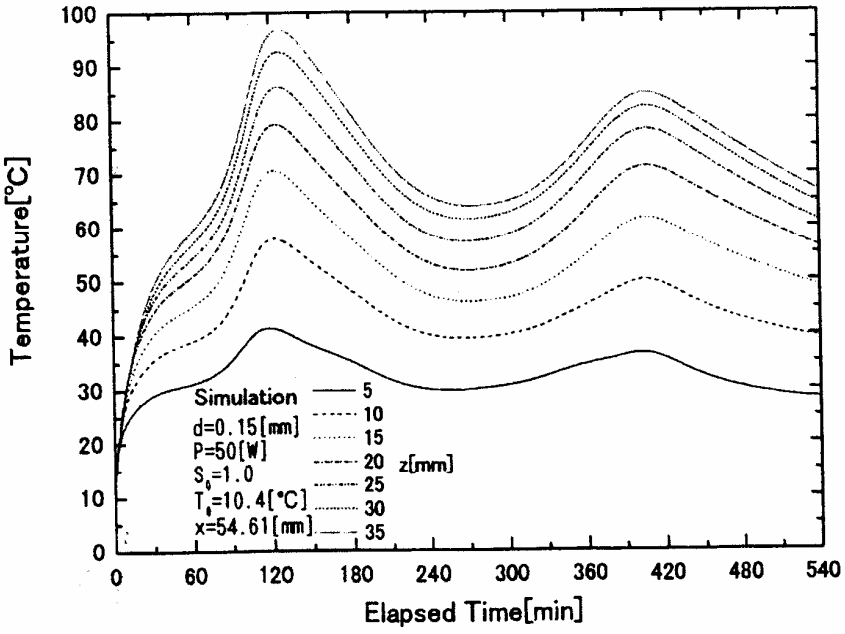

FIGURE 8: Temperature profile in times at various depths (P=50 W, d=0.15 mm, s_0 = 1.0): (a) Experiment; (b) Simulation

which corresponds to that of microwave power level of 50 (W) and initial temperature of 10. 5 (°C), along with the center axis (x=54.61 mm) of rectangular wave guide.

Figure 8 shows the temperature profiles at various times and depths in the case of s=1.0 and d=0.15(mm). It is seen that the temperature profiles within the sample steady rise in the early stages of drying (about 90 minutes), however, the temperature in the interior of the sample are higher than those at the drying surface for all times during the drying process. Due to the large initial moisture content, the skin-depth heating effect causes a major part of incident wave to be reflected from the surface. The latter arises from the fact that the microwave power absorbed in the interior is lowest. As the drying process proceeds (about 90-240 min), after a majority of moisture content has been removed from the sample, the large part of microwaves can penetrate further into the sample as material dries where the strength of the microwave power absorbed within the sample increases. During this stage, the behavior of dielectric properties is influenced primarily by that of moisture content, and heating becomes more volumetric. In time about 240 minutes, the temperature starts to drop, this is mainly due to fact that the moisture inside the sample is significantly reduced, reducing the microwave power absorbed within the sample.

However, at long drying times (about 480 min), the inside temperature increases again due to the characteristic of dielectric loss factor, which becomes to dominate microwave drying at low moisture contents where the reflection and transmission components of microwave at each interface will contribute to the stronger standing waves patterns within the sample. Further, near the end stages of drying as the majority of moisture content inside the sample has been removed, this decreases the microwave power absorbed. Thus, equilibrium is reached between microwave drying and convective losses by lowering the sample temperature. The simulated results are in agreement with the experimental results for microwave drying.

Figure 9 shows the temperature profiles at various times and depths in the case of s_0=0.6 and d=0.15(mm). In this case, the sample dries quickly throughout, and the temperature profiles within the sample rise up rapidly in the early drying times (about 27 minutes). This is because of the total rate of reflected wave is small in the early drying times, and a large part of microwaves penetrates further into the sample compared with the previous cases (as referred to Figure 8). Such pattern can lead to a much higher rate of microwave power absorbed in the interior. After this, the temperature starts to drop continuously, because of the rate of microwave power absorbed is lower after a majority of moisture content has been removed from the sample. Continued drying process (about 240 minutes) would cause the temperature level to increase again due to the characteristic of the dielectric loss factor that was explained in Figure 8. The simulated results are in agreement with the experimental results for microwave drying.

Figure 10 shows the temperature profiles at various times and depths in the case of s_0=1.0 and d=0.4 mm. Since the large particle size corresponds to a lower dielectric loss factor, a larger part of microwave can penetrate further into the sample. The reflection and transmission components at each interface, air to upper surface of sample and lower surface of sample to air, will contribute to standing wave configuration inside the sample. Such configuration can lead to a much higher microwave power absorbed or heat generation rate in the interior. Consequently, the temperature profiles now appear uniform shape close to the entire interior section of the board located midway between the half of sample depth and lower surface where there is the most moisture content.

Figure 11 shows the temperature profiles at various times and depths in the case of s_0=1.0 and d=1.0 mm. As the drying continues, the temperature profiles within the sample are different from those shown in previous cases. In this case, the temperature profiles have a rather unusual shape. This is because of the large particle size corresponding to a lower capillary pressure, the liquid water supply to surface by capillary action become insufficient to replace the liquid being evaporated. The latter arises from the fact that the dry layer took place over small effective surface or on a front retreating from the surface into the interior of the sample dividing it into two regions, dries region and wet region. Inside the drying front, the sample is wet, i.e. the voids contain liquid water and the main mechanism of moisture transfer is capillary pressure. Outside the

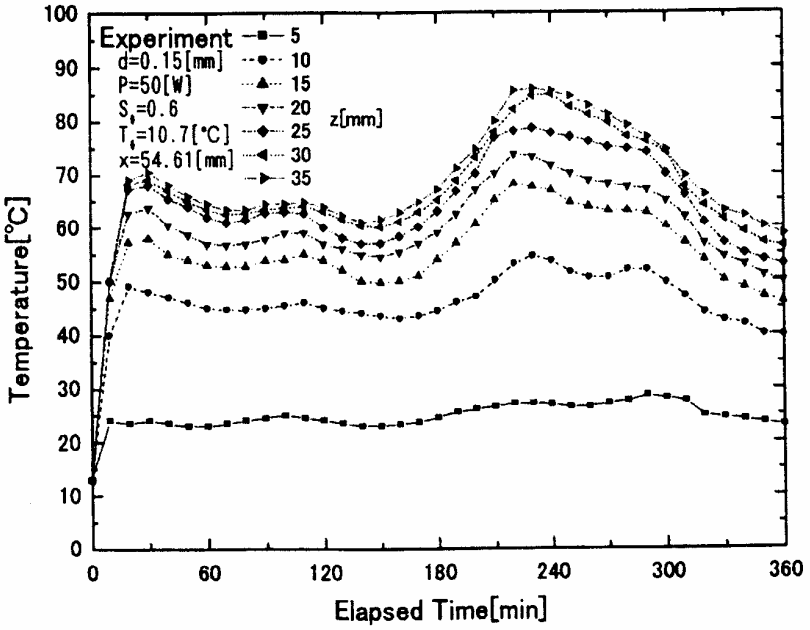

(a)

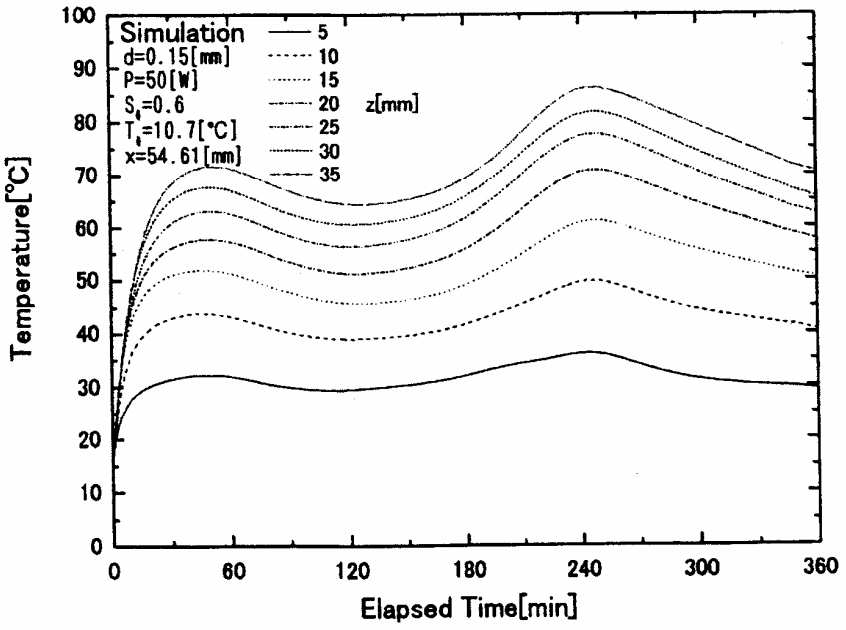

(b)

FIGURE 9: Temperature profile in times at various depths (P=50 W, d=0.15 mm,s_0=0.6): (a) Experiment; (b) Simulation

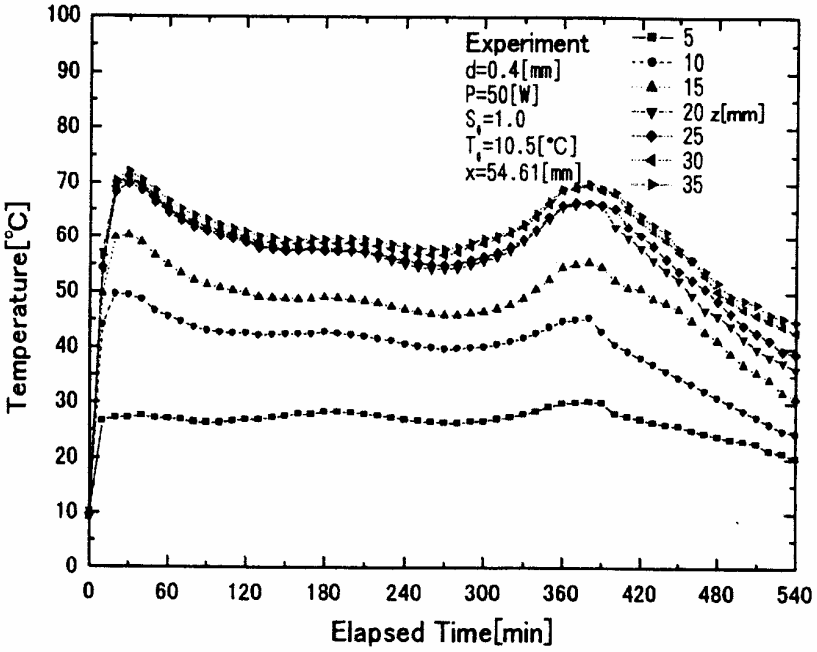

(a)

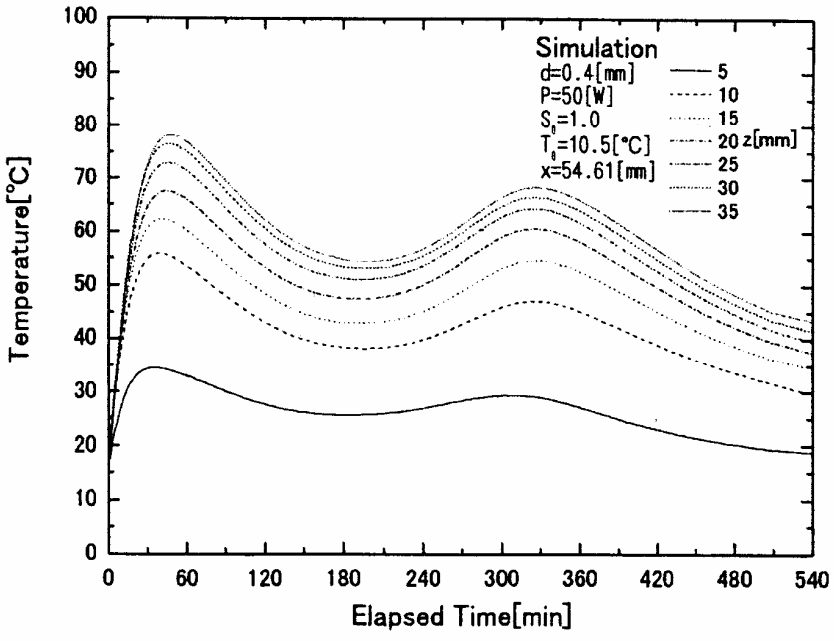

(b)

FIGURE 10: *Temperature profile in times at various depths (P=50 W, d=0.4 mm,s_0=1.0): (a) Experiment; (b) Simulation*

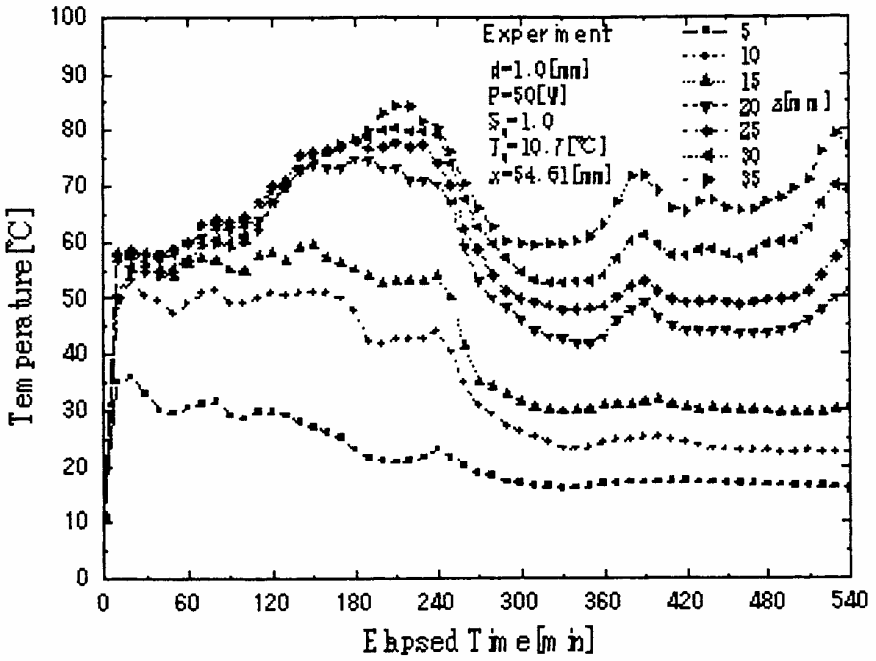

FIGURE 11: Temperature profile in times at various depths (Experiment: P=50 W, d=1.0 mm,s_0=1.0).

drying front, no liquid water exists, all water is in vapor state and the vapor diffusion plays an important role in the moisture migration mechanism.

Furthermore, the combination of characteristic of hydrodynamic and dielectric properties would change the location of maximum temperature with respect to times especially, at the drying times about 45 min-180 min. This trend is more remarkable for large particle sizes. Unfortunately, the lack of experimental data (permabilities and capillary pressure functions) for a large particle sizes, therefore, the drying kinetics predicted by the mathematical model were unrepresentative.

The observation of temperature profiles depicted in Figures 8-10 for the sample verify that the match between the simulated results and experimental data is qualitatively consistent, with the simulated results exhibiting the same overall trend of the experimental profiles. However, there are some differences in the maximum temperature between the simulated results and experimental data, see Figures 8 and 10. The discrepancy may be attributed to uncertainties in the thermal and dielectric property database. In addition, the discrepancy may be attributed from the nonuniformity of the microwave irradiation during experimental process.

Furthermore, the simulation and experimental data of temperature distributions within the sample in the vertical plane (x-z) are compared in Figures 12-14. The result shows the greatest temperature in the center of heating sample (which corresponds to a higher microwave power absorbed) with the temperature decreasing towards the side walls of the sample. It can be seen that the agreement between the two heating patterns is good, particularly concerning the location of the hot region.

Distribution of Moisture Profiles Within the Sample

Figure 15 shows the average moisture profile along the sample depth in the case of s_0=1.0 and d=0.15(mm). In the early drying times, the moisture content at the leading edge of the sample is lower than that inside the sample, where the moisture decreases due to the gravitational effect. Since the higher moisture content, much larger reflected waves develop from the surface during the early stages of drying. Later, the surface of the sample is supplied with liquid water through gradient in the capillary pressure, and because of the condensation of water vapor (which moves towards the surface due to a gradient in the vapor partial pressure), due to the lower temperature of the surface. At this stage, how-

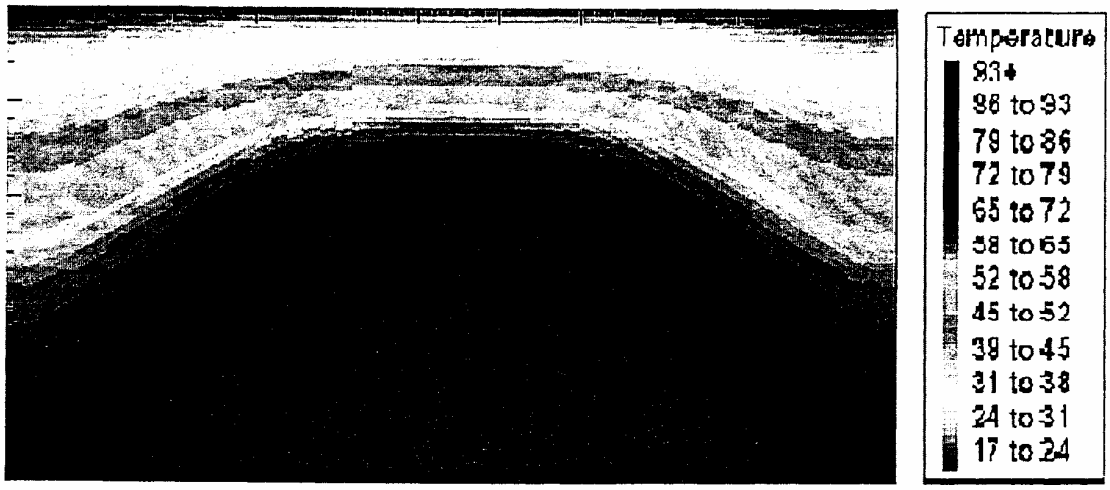

(a)

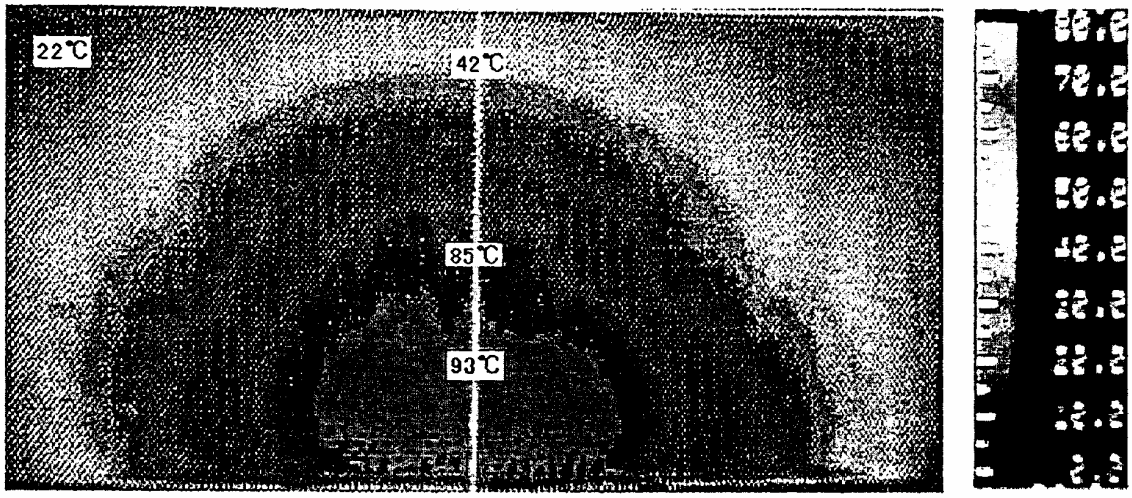

(b)

FIGURE 12: *Comparison between simulated results (a) and experimental results (b) for microwave drying of initial saturated sample (t=120 min, d=0.15 mm, s_0=1.0).*

ever, the internal moisture content transfer is mainly attributable to capillary flow of liquid water through the voids.

Continued drying process would cause the average moisture content inside the sample to decrease and lead to decreased microwave power absorbed, reduced temperature and evaporation rate.

Nevertheless, at the longer drying times, the vapor diffusion effect plays an important role in the moisture migration mechanism because of the sustained vaporization that is generated within the sample. The simulated results are in agreement with the experimental results for microwave drying.

Figure 16 shows the average moisture profile along the sample depth in the case of s_0=0.6 and d=0.15(mm). It is evident from the figure that the sample dries quickly throughout. In particular, the bulk of this sample that receives the largest amount of microwave power absorbed (which corresponds to a small initial moisture content) in the early stages of drying times, due to the penetration depth of the microwave field. In this case, the vapor diffusion

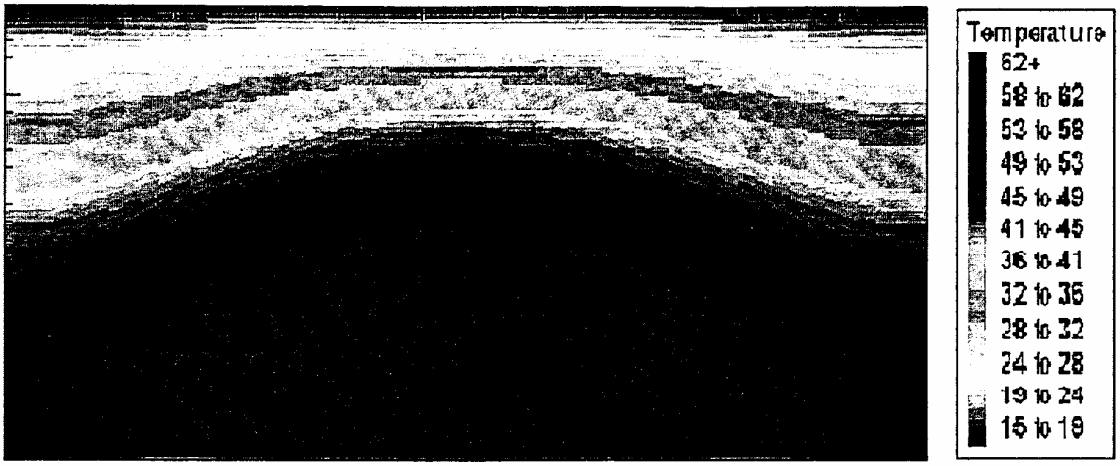

(a)

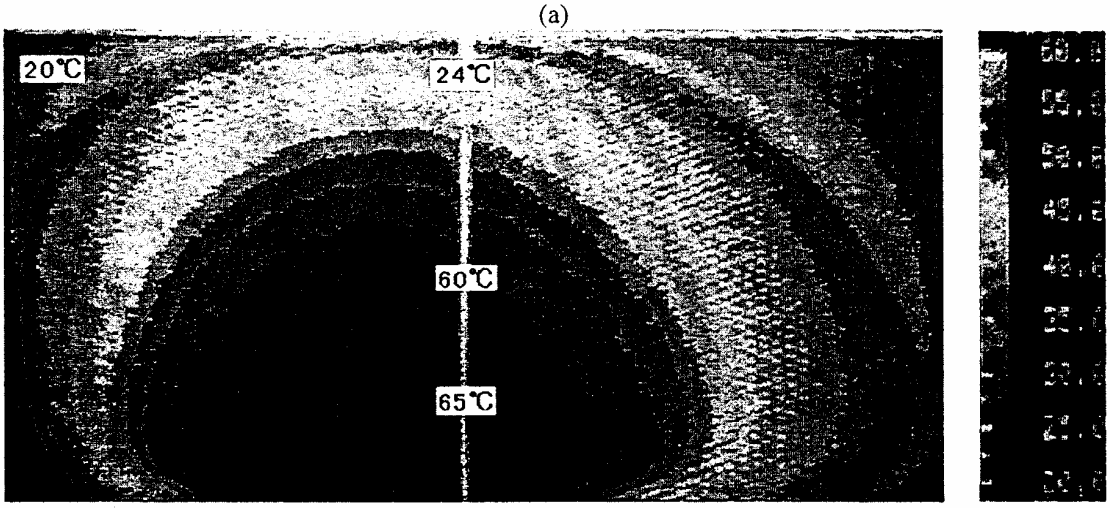

(b)

FIGURE 13: *Comparison between simulated results (a) and experimental results (b) for microwave drying of initial partially saturated sample (t=120 min, d=0.15 mm, s_0=0.6)*

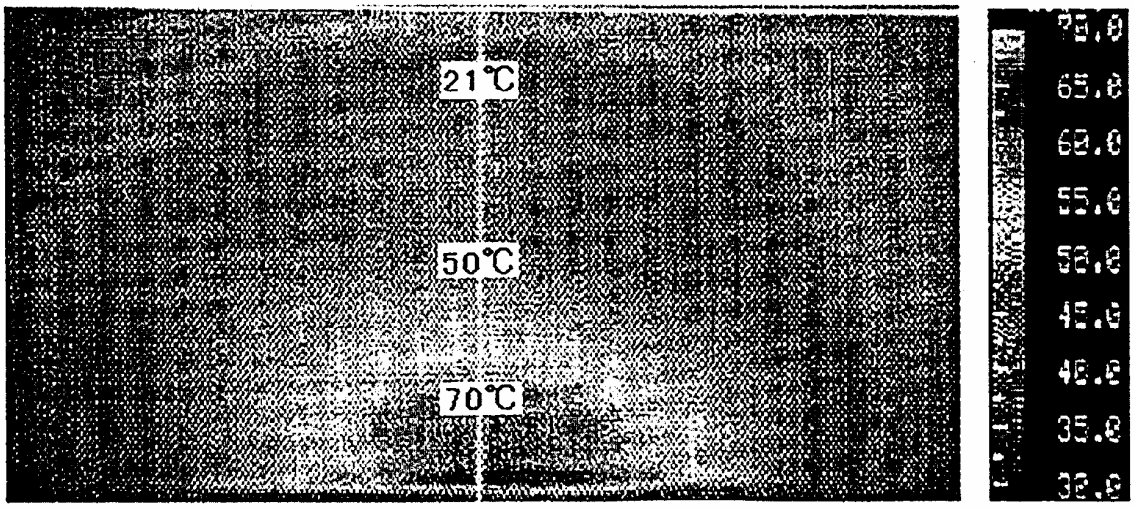

FIGURE 14: *Experimental results for microwave drying of initial saturated sample (t=360 min, d=1.0 mm, s_0=1.0).*

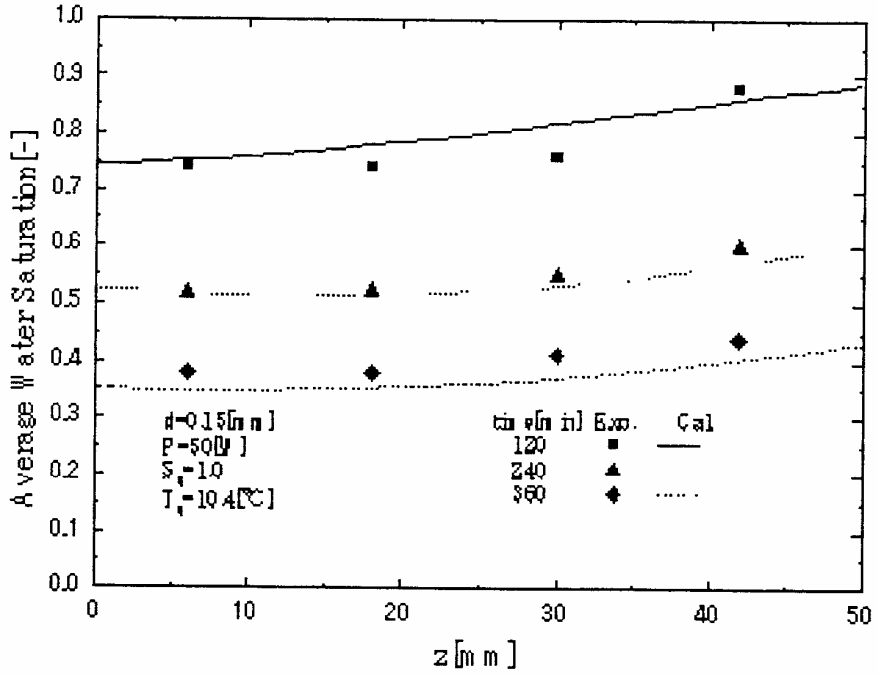

FIGURE 15: Average water saturation as a function of depth at various times (P=50W, d=0.15 mm, s_0=1.0).

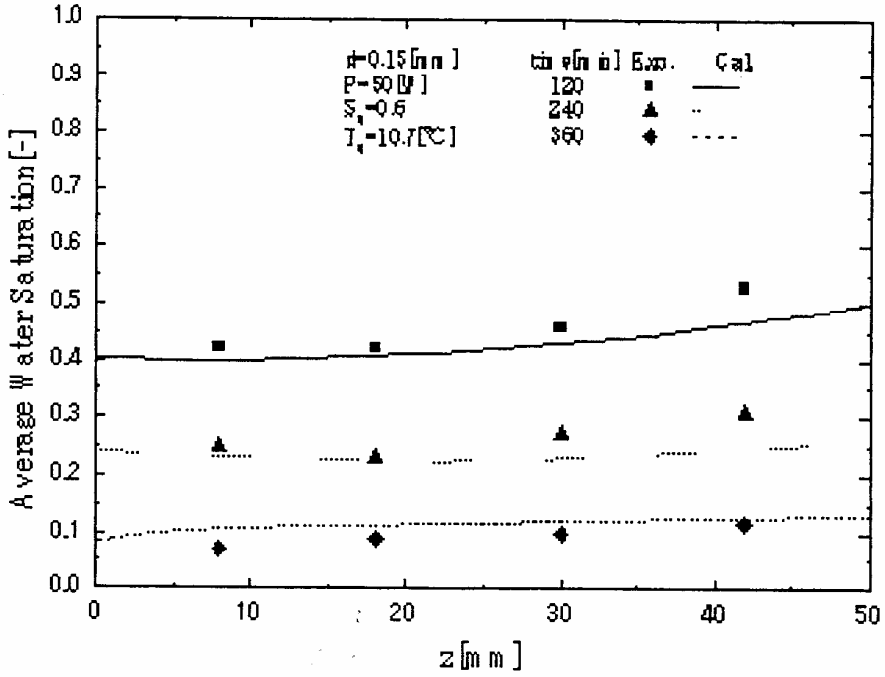

FIGURE 16: Average water saturation as a function of depth at various times (P=50W, d=0.15 mm, s_0=0.6).

plays an important role in the moisture migration mechanism. The simulated results are in agreement with the experimental results for the microwave drying process.

The simulations of moisture distribution within the sample in the vertical plane (x-z) are shown in Figures 17 and 18. It is seen that the moisture content now appears to be high close to side walls of the sample, and the moisture content at lowering edge of the sample stays higher due to the stronger gravitational effect.

The following discussion refers to the effect of particle sizes on the microwave drying kinetics under same conditions. The distribution of average moisture profiles for different values of particle sizes (d=0.15 mm and d=0.4 mm) with the same microwave power level (P=50 W) at the same time is presented in Figure 19. The observed moisture content profiles at the leading edge of the sample in the case of small particle sizes are higher than that case of large particle sizes. This is because of the small particle size which corresponds to a higher capillary pressure can cause moisture to reach the surface at a higher rate than in the case of large particle sizes. On the other hand, in the case of large particle sizes, the moisture profiles at the leading edge of the sample are always lower due to the lower capillary pressure in comparison to the case of small particle sizes.

Furthermore, the variation of drying rate with respect to time is shown in Figure 20. It is seen that in the early drying times, the drying rate of the sample in the case of small particle sizes is nearly the same in that case of large particle sizes. This is because the drying rate is nearly independent of the capillary porous materials being dried. However, at longer drying times, the observed drying rate of sample in the case of small particle sizes is higher than that case of large particle sizes. This is because the small particle sizes lead to much higher capillary force resulting in a faster drying time and more uniform moisture profile along the sample.

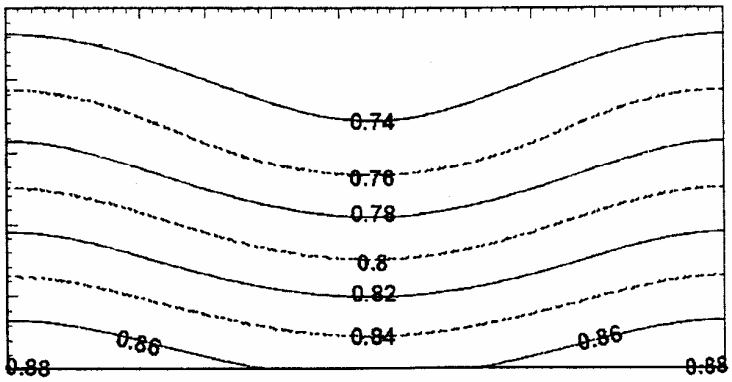

FIGURE 17: The simulated water saturation distributions (dimensionless) within the sample (s_0=1.0, time=120 min, d=0.15mm).

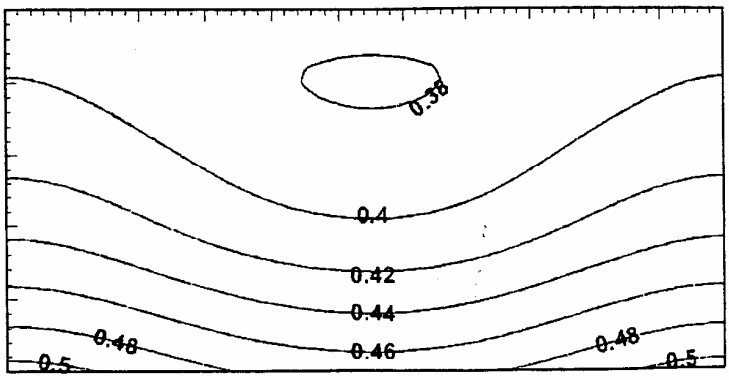

FIGURE 18: The simulated water saturation distributions (dimensionless) within the sample (s_0=0.6, time=120 min, d=0.15mm).

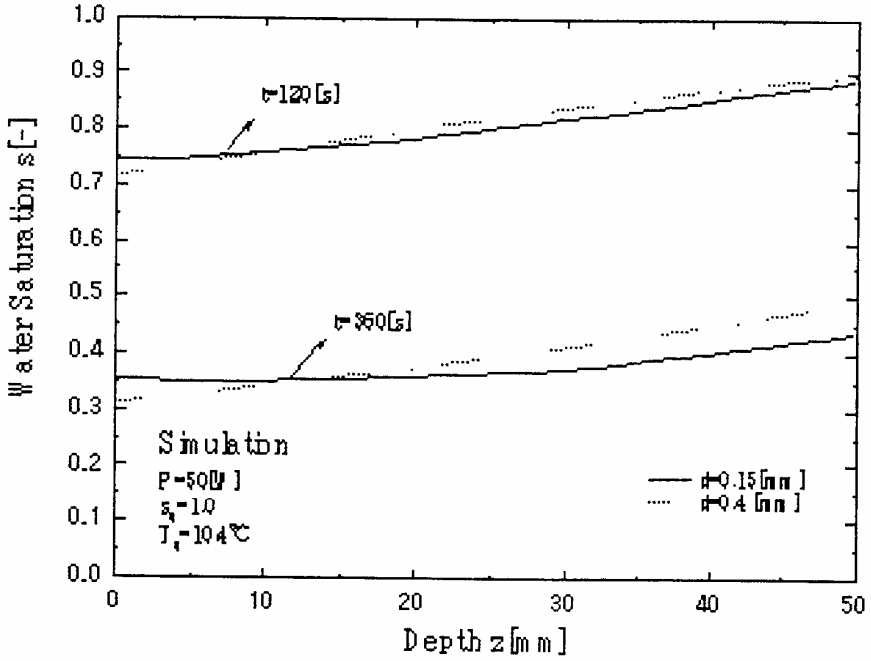

FIGURE 19: The comparison of average water saturation as a function of depth at various particle sizes (P=50W, s_0=1.0).

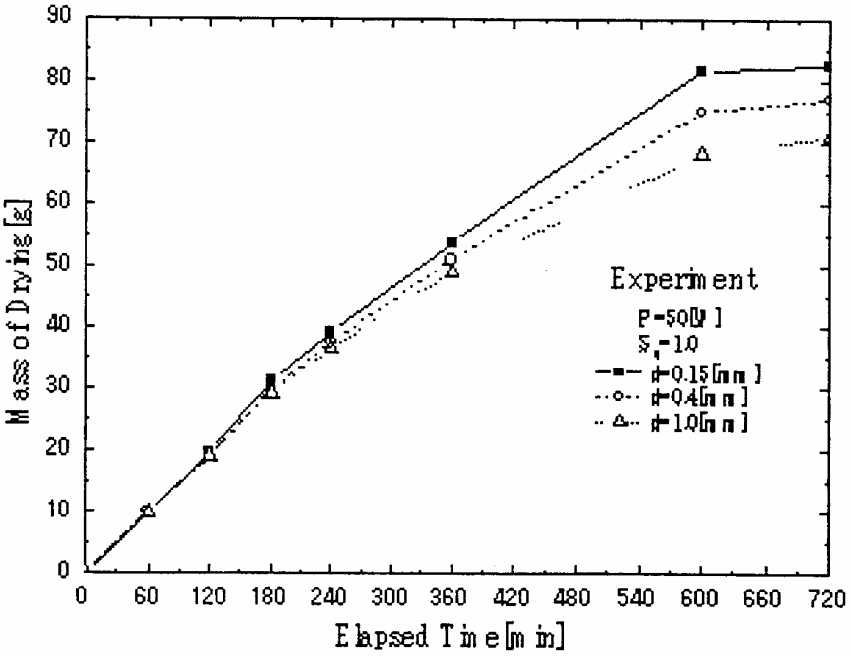

FIGURE 20: The variation of drying rate with respect to time.

Finally, from this study, the capability of the mathematical model to correctly handle the field variations at the interfaces between materials of different dielectric properties was shown. With further quantitative validation of the mathematical model for microwave drying using a rectangular wave guide, it is clear that the model can be used as a real tool for investigating in detail this particular microwave drying of porous material at a fundamental level.

Conclusions

The experiments and theoretical analysis presented

in this paper describe many of the important interactions within a capillary porous medium during microwave drying using a rectangular wave guide. The following summarizes the conclusions of this work:

1. A generalized mathematical model of drying process by microwave using rectangular wave guide is proposed. It is used successfully to describe the drying phenomena under various conditions.
2. The calculations of electromagnetic fields inside the rectangular wave guide and the sample showed that the variation of particle sizes and initial moisture content changes the degree of penetration and rate of heat generation within the sample. This is because of the dielectric properties of material strongly affects the electromagnetic field and the characteristics of the dielectric properties are influenced primarily by that of moisture content and temperature distributions within the sample.
3. The differences of the drying kinetics for the cases of small particle and large particle sizes were clarified in detail, relating to the interference between the characteristics of dielectric properties (dielectric loss factor and loss tangent coefficient) and hydrodynamic properties (capillary pressure, vapor diffusion and gravitational force) in the sample. The small particle size leads to much higher capillary forces resulting in a faster drying time.
4. At longer drying times, the inside temperature increases again due to the characteristic of dielectric loss factor, which becomes to dominate microwave drying at low moisture contents where the reflection and transmission components of microwave at each interface will contribute to the stronger standing waves patterns within the sample. This phenomenon commonly referred to as thermal runaway. During this stage, poor product quality and sample cracking are often exhibited (especially, for very fine matrix sample such as heavy clay and timbers) if temperature levels and distribution cannot be controlled. Understanding, prediction, and preventing or controlling thermal runaway present a major challenge to the development of microwave processing.
5. A more general observation concerning the moisture profiles for many materials pertains to the effect of matrix structure (particle sizes or pore sizes) on the mechanism of moisture movement. From a macroscopic point of view, the ease with which the water can move in the liquid phase depends on the nature of the matrix structure within the materials. In truly capillary porous materials, a natural redistribution of the moisture from within the materials as the surface water evaporates. However, many materials have structures in which the pores are too large or discontinuous for this to take place. In other materials, the water is held in a matrix which makes water liquid movement impossible.
6. Finally, our future aim is to validate the investigation of microwave drying process of multilayered capillary porous materials, as well as, the full comparison between mathematical model prediction and experimental data.

Acknowledgment

We would like to than the reviewers for their constructive comments.

Nomenclature

B	magnetic flux density [Wb/m^2]
C_p	specific heat capacity [J/kgK]
D	electric flux density [C/ m^2]
D_0	binary mass diffusion coefficient [m^2/s]
d	diameter [m]
E	electric field intensity [V/m]
E_{yin}	the input value of electric field intensity [V/m]
f	frequency of incident wave [Hz]
g	gravitational constant [m/s^2]
H	magnetic field intensity [A/m]
h_c	heat transfer coefficient [W/m^{2}K]
h_m	mass transfer coefficient [m/s]
H_v	specific heat of vaporization [J/kg]
K	permeability [m^2]
L_x	the length of wave guide in x-direction [m]
$\dot{n}$	volumetric evaporation rate [kg/m^{3}s]
P	microwave power level [W]
p	pressure [Pa]
Q	microwave power absorbed term [W/m^3]

q	heat flux [W/ m^2]
R	universal gas constant [J/mol/K]
s	water saturation
T	temperature [°C]
tan δ	dielectric loss tangent coefficient
t	time [s]
U_∞	air velocity [m/s]
u, w	velocity [m/s]
Z_H	wave impedance [Ω]
Z_I	intrinsic impedance [Ω]

Greek letters

ϕ	porosity [m^3/ m^3]
ρ	density [kg/m^3]
ε	permittivity [F/m]
ε_r	relative permittivity or relative dielectric constant
ε_0	permittivity in free space [F/m]
λ_0	free space wave length [m]
λ_g	waveguide wave length [m]
λ_{eff}	effective thermal conductivity [W/mK]
μ	magnetic permeability [H/m]
μ_g	dynamic viscosity of gas [Pa s]
μ_l	dynamic viscosity of liquid [Pa s]
υ	velocity of microwave [m/s]
σ	electric conductivity [S/m]
ξ	surface tension [Pa m]

Subscripts

∞	ambient
0	free space
a	air
c	capillary
c	effective
g	gas
ir	irreducible
n	component of normal direction
p	particle
r	relative
t	component of tangent direction
v	water vapor
l	liquid water
x, y, z	coordinates

Superscripts

'	interfacial position

References

Ayappa, K.G., Davis, H.T., Crapiste, G., Davis, E.A. and J. Gordon. 1991. Microwave Heating: An Evaluation of Power Formulations. Chemical Engineering Science 46: 1005-1016.

Bories, S.A. 1991. Fundamental of Drying of Capillary-Porous Bodies, in Kakac, S., Kilkis, B., Kulacki, F. and Arinc, F. (Ed.), Convective Heat and Mass Transfer in Porous Media, NATO ASI series Vol. 196, Kluwer Publishers: 39-434.

Chen, P. and Schmidt, P.S. 1990. An Integral Model for Drying of Hygroscopic and Nonhygroscopic Materials with Dielectric Heating. Drying Technology 8: 907-930.

Clemens, J. and Saltiel, C. 1996. Numerical Modeling of Materials Processing in Microwave Furnaces. Int. J. Heat and Mass Transfer 39 (8): 1665-1675.

Constant, T., Moyne, C. and Perre, P. 1996. Drying with Internal Heat Generation: Theoretical Aspects and Application to Microwave Heating. AIChE J. 42 (2): 359-368.

Gori, F., Gentili, G. and Matini, L. 1987. Microwave Heating of Porous Media. ASME J. Heat Transfer 109: 522-525.

Metaxas, A.C. and Meridith. R.J. 1983. Industrial Microwave Heating. Peter Peregrinus, Ltd., London.

Mur, G. 1981. Absorbing Boundary Conditions for the Finite-Difference Approximation of the Time-Domain Electromagnetic-Field Equations. IEEE Transactions of Electromagnetic Compatibility EMC-23 (4): 377-382.

Ni, H., Datta, A. and Torrance, K.E. 1999. Moisture Transport in Intensive Microwave Heating of Biomaterials: A Multiphase Porous Media Model. Int. J. Heat and Mass Transfer 42: 1501-1512.

Patankar, S.V. 1980. Numerical Heat Transfer and Fluid Flow. Hemisphere Publishing Corporation, New York.

Perkin, R.M. 1980. The Heat and Mass Transfer Characteristics of Boiling Point Drying Using Radio Frequency and Microwave Electromagnetic Fields. Int. J. Heat and Mass Transfer 23: 687-695.

Perre, P. and Turner, I.W. 1997. Microwave Drying of Softwood in an Oversized Waveguide. AIChE

J. 43(10): 2579-2595.

Ratanadecho, P., Aoki, K. and Akahori, M. 2001(a). Experimental and Numerical Study of Microwave Drying in Unsaturated Porous Material, Int. Comm. Heat and Mass Transfer 28(5): 605-616.

Ratanadecho, P., Aoki, K. and Akahori, M. 2001(b). A Numerical and Experimental Investigation of the Modelling of Microwave Melting of Frozen Packed Bed Using a Rectangular Wave Guide. Int. Commun. Heat Mass Trans 28(6): 751-762.

Ratanadecho, P., Aoki, K. and Akahori, M. 2001(c). A Numerical and Experimental Study of Microwave Drying Using a Rectangular Wave Guide. Drying Technology J. 19(9): 2209-2234.

Ratanadecho, P., Aoki, K. and Akahori, M. 2002. A Numerical and Experimental Investigation of the Modeling of Microwave Heating for Liquid Layers Using a Rectangular Wave Guide (Effects of Natural Convection and Dielectric Properties). Appl. Math. Modelling 26(3):449-472.

Rogers, J.A. and Kaviany, M. 1992. Funicular and Evaporative-Front Regimes in Convective Drying of Granular Beds. Int. J. Heat and Mass Transfer 35 (2): 469-479.

Saltiel, C. and Datta, A. 1997. Heat and Mass Transfer in Microwave Processing. Adv. Heat Transfer 30:1-94.

Turner, I.W. and Jolly, P.J. 1990. The Effect of Dielectric Properties on Microwave Drying Kinetics. J. Microwave Power and Electromagn. Energy 25: 211-223.

Turner, I.W. and Jolly, P.J. 1991. Combined Microwave and Convective Drying of a Porous Material. Drying Technology 9(5): 1209-1269.

Turner, I.W., Puiggali, J.R. and Jomaa, W. 1998. A Numerical Investigation of Combined Microwave and Convective Drying of a Hygroscopic Porous Material: A Study Based on Pine Wood. Trans IChemE 76:193-209.

Wang, J. and Schmugge, T. 1980. An Empirical Model for the Complex Dielectric Permittivity of Soil as a Function of Water Content. IEEE Transactions on Geosciences and Remote Sensing GE-18 (4): 288-295.

Wei, C.K., Davis, H.T., Davis, E.A. and Gordon, J. 1985. Heat and Mass Transfer in Water-Laden Sand Stone: Microwave Heating. AIChE J. 31 (5): 842-848.

Whitaker, S. 1977. A Theory of Drying in Porous Media. Adv. Heat Transfer 13: 119-203.